



# Parameter Optimization of Eel Robot Based on NSGA-II Algorithm

AnFan Zhang<sup>1</sup>(✉), Shugen Ma<sup>2</sup>, Bin Li<sup>3</sup>, MingHui Wang<sup>3</sup>, and Jian Chang<sup>3</sup>

<sup>1</sup> Faculty of Marine Science and Technology,  
Hainan Tropical Ocean University, Sanya, China  
zhangaf@hntou.edu.cn

<sup>2</sup> Department of Robotics, Ritsumeikan University, Shiga-ken 525-8577, Japan

<sup>3</sup> State Key Laboratory of Robotics, Shenyang Institute of Automation,  
Chinese Academy of Sciences, Shenyang, China

**Abstract.** In order to obtain an efficient gait, this paper studies the swimming efficiency of underwater eel robot in different gaits. The optimal gait parameters combination of three gaits is studied by using Non-dominated Sorting in Genetic algorithm (NSGA-II). The relationship between input power and velocity in different gait patterns is analyzed, and the optimal gait parameters combination in each gait patterns is obtained. The simulation results show that the new gait only need less input power than the serpentine gait in the same velocity, and the new gait has faster velocity compared to the eel gait using the same joint input power. Finally, the above founds have further verified by experiments. The experiments have proved that the new gait has higher swimming efficiency. Besides, It is found that both the optimal gait amplitude and optimal phase shift exist in both the new gait and the serpentine gait.

**Keywords:** Parameter optimization · Gait pattern · NSGA-II · Eel robot

## 1 Introduction

High efficiency gait will help the energy utilization of the robot and prolong the working time of the robot. One approach to obtain an efficient gait is by deriving an analytical solution of the optimal gait. However, the eel robot system is a highly coupled and the number of the system states increases with the increase of the number of modules, which makes it difficult to obtain the analytical solution of the optimal gait. An even more main approach called numerical analysis method [1–3] can be divided into two approaches according to the models of robot and usually contains a serial of assumptions [4]. One is based on CPG model. The amphibious snake-like robot adopted a gradient-free online Powell method combined with CPG model to obtain the optimal gait [5]. The advantages of this method are low computational cost and fast speed, but the parameters of CPG model lack physical significance. The other is the gait optimization based on the

dynamic model, and the physical meaning of the model parameters is obvious. This paper mainly studies the optimal gait problem based on the dynamic model of underwater eel-like robot.

The eel-like robot belongs to a chain-like structure robot without a fixed base. There are many related studies on gait optimization of chain-structured robot without fixed base on land or amphibious [5–9]. It can be divided into two categories. The first type uses optimal control method to obtain optimal gait. Ostrowski [2] elaborated the gait selection and optimal control of nonholonomic motion system with Lie group symmetry. Lagrange reduction theory was used to simplify the optimal control problem. Optimal control technology was used to study the optimal gait and gait shifting, but the computational cost of this technology is high. In order to reduce the computational complexity, Cortes [10] studied the optimal control and gait selection of dynamic systems with group symmetry. The truncated basis function with periodic input was used to obtain the solution of the approximate optimal control problem, but only the approximate optimal gait of eel-like robot was studied. The second method is to obtain the optimal gait parameter combination by using optimization algorithm. Parodi [11] used Lyapunov method to design the controller to ensure that the body shape converges to local curvature. The locally optimized gait parameters ensured rapid system response and efficient propulsion. The evaluation indicator was used to evaluate the energy and rapid response ability.

In [12, 13], The NSGA-II algorithm was used to analyze the optimal gait parameter combination of land snake-like robot, and only serpentine gait pattern was analyzed, no attention is paid to other gait patterns. The optimal gait amplitude parameter was concentrated around  $\alpha \sim 30^\circ$  and the optimal gait phase shift was concentrated around  $\beta \sim 70^\circ$  of land snake-like robot are obtained. Compared with the force that the robot receives on the land, hydrodynamic force that the robot receives under water is more complex, its feasible gait space is more diverse than the terrestrial environment, and the solution space to be searched is larger. In [1], the Particle Swarm Optimization (PSO) and genetic algorithm (GA) were used to optimize the parameter combination of serpentine gait. Multi-objective optimization algorithm MOO was adopted to optimize the gait parameters combination of serpentine gait [3]. Kelasidi [14] studied the relationship between gait parameters, forward speed and power consumption in two gaits (eel gait and serpentine gait), and found that the power consumption COST per unit mass decreased with the increase of modules, but the average power used cannot reflect the change of instantaneous power.

This paper analyzes the relationship between the input power, velocity and gait parameters of the underwater eel robot in new gait (found in [15]), eel gait, serpentine gait. The advantages and disadvantages of the new gait are emphatically analyzed compared with the other two gaits. The energy efficiency of the three gait is analyzed and compared by using the dynamic model in non-inertial frame and the multi-objective optimization algorithm NSGA-II. The analytical dynamic model based on non-inertial frame is used to calculate dynamics, which can effectively reduce the computation time of dynamics. The multi-objective optimization NSGA-II algorithm is used to effectively reduce the calculation

time and quickly find the Pareto frontier, so as to improve the calculation efficiency. The two optimal objectives are the minimum power input and the maximum velocity. Taking the sum of the maximum input power plus absolute value as input power can effectively prevent the situation of excessive instantaneous power. The simulation results show that the eel-like robot with the new gait consumes less power than that of the serpentine gait and eel gait at the same speed, and has faster speed at the same input power. Finally, experiments verify the efficiency of the new gait, and the relationship between the average speed and the gait amplitude and the phase shift in the new gait and serpentine gait is analyzed.

## 2 The Dynamic Model of the Eel Robot

In this paper, the dynamic model in [17] is adopted, which is based on a special non-inertial system. Considering only two-dimensional motion, it is assumed that the eel robot is buoyancy-gravity equilibrium, and that the robot is a slender body with circular cross-section.

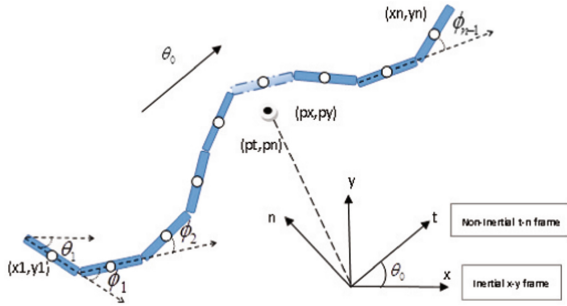


**Fig. 1.** The prototype of underwater Eel-like robot and its kinematic parameters.

The kinematics of the planar eel robot is presented and illustrated in Fig. 1 consisting of  $n$  links of length  $2l$  interconnected by  $n - 1$  active joints. The robot is defined with respect to the fixed global frame,  $x - y$ , and is still defined with respect to the non-inertial  $t - n$  frame, and both of them share the same origin (Fig. 1). Each link has the same mass  $m$ , moment of inertia  $\frac{1}{3}ml^2$  and the  $x_i - y_i$  frame attached to the mass center of each link. The mathematical symbols are described in Table 1. The joint angle vector is defined as  $\phi = [\phi_1, \phi_2, \dots, \phi_{n-1}]^T$ , and absolute angle in global frame is defined as  $\theta = [\theta_1, \dots, \theta_n]^T$ , orientation angle is defined as  $\theta_0 = \frac{1}{n} \sum_1^n \theta_i$ . Correspondingly absolute angle in  $t-n$  frame is  $\Phi = [\Phi_1, \dots, \Phi_n]^T$ . The direction of the  $t$  axis is along eel robot tangential or forward direction, and the direction of the  $n$  axis is along the normal direction of the robot.  $\theta_0 \in R$  stands for the global frame orientation and is expressed with respect to the global  $x$  axis with counterclockwise positive direction. Other coefficients are defined by

**Table 1.** Definition of mathematical terms

Symbol	Definition
$n$	The number of links
$m$	Link mass
$\theta$	Absolute angle vector in global frame
$\phi$	Joint angle vector
$\theta_0$	Orientation angle of Eel robot
$\boldsymbol{\theta}$	Absolute angle vector in global frame
$\boldsymbol{\phi}$	Joint angle vector
$\boldsymbol{\Phi}$	Absolute angle vector in t-n frame
$\alpha$	Gait amplitude
$\omega$	Gait frequency
$\beta$	Phase shift
$\gamma$	The offset of the joint angle

$$\begin{aligned}
\mathbf{A} &= [\mathbf{I}_{n-1}, \mathbf{0}_{n-1}] + [\mathbf{0}_{n-1}, \mathbf{I}_{n-1}] & \mathbf{e} &= [1 \dots 1]^T \\
\mathbf{D} &= [\mathbf{I}_{n-1}, \mathbf{0}_{n-1}] - [\mathbf{0}_{n-1}, \mathbf{I}_{n-1}] & \mathbf{K} &= \mathbf{A}^T (\mathbf{D}\mathbf{D}^T)^{-1} \mathbf{D} \\
\mathbf{V} &= \mathbf{A}^T (\mathbf{D}\mathbf{D}^T)^{-1} \mathbf{A} & \mathbf{J} &= \mathbf{J}\mathbf{I}_{n,n} \\
\sin \boldsymbol{\Phi} &= [\sin \Phi_1, \dots, \sin \Phi_n]^T & \mathbf{S}_{\boldsymbol{\Phi}} &= \text{diag}(\sin(\boldsymbol{\Phi})) \\
\cos \boldsymbol{\Phi} &= [\cos \Phi_1, \dots, \cos \Phi_n]^T & \mathbf{C}_{\boldsymbol{\Phi}} &= \text{diag}(\cos(\boldsymbol{\Phi})) \\
\mathbf{W}_c &= [\mathbf{B}_m, \mathbf{e}] = \begin{bmatrix} \mathbf{D} \\ \mathbf{e}^T/n \end{bmatrix}^{-1} & \mathbf{E} &= \begin{bmatrix} \mathbf{e} & \mathbf{0}_{n \times 1} \\ \mathbf{0}_{n \times 1} & \mathbf{e} \end{bmatrix} \\
\mathbf{R}_{2n \times 2n} &= \begin{bmatrix} \cos \theta_0 \mathbf{I}_{n,n} & \sin \theta_0 \mathbf{I}_{n,n} \\ -\sin \theta_0 \mathbf{I}_{n,n} & \cos \theta_0 \mathbf{I}_{n,n} \end{bmatrix} & \boldsymbol{\theta} &= \mathbf{W}_c \begin{bmatrix} \boldsymbol{\phi} \\ \theta_0 \end{bmatrix}.
\end{aligned}$$

The fluid force model adopted in this dynamic model considers linear resistance, additional mass force effect, non-linear resistance and fluid moment. The acceleration of the CM in t-n frame can be expressed as

$$\begin{aligned}
\begin{bmatrix} \dot{v}_t \\ \dot{v}_n \end{bmatrix} &= -M_p \begin{bmatrix} u_n \mathbf{e}^T \mathbf{S}_{\boldsymbol{\Phi}}^2, -u_n \mathbf{e}^T \mathbf{S}_{\boldsymbol{\Phi}} \mathbf{C}_{\boldsymbol{\Phi}} \\ -u_n \mathbf{e}^T \mathbf{S}_{\boldsymbol{\Phi}} \mathbf{C}_{\boldsymbol{\Phi}}, u_n \mathbf{e}^T \mathbf{C}_{\boldsymbol{\Phi}}^2 \end{bmatrix} \left( \begin{bmatrix} l \mathbf{K}^T \mathbf{S}_{\boldsymbol{\Phi}} \ddot{\boldsymbol{\Phi}} + l \mathbf{K}^T \mathbf{C}_{\boldsymbol{\Phi}} \dot{\boldsymbol{\Phi}}^2 \\ -l \mathbf{K}^T \mathbf{C}_{\boldsymbol{\Phi}} \ddot{\boldsymbol{\Phi}} + l \mathbf{K}^T \mathbf{S}_{\boldsymbol{\Phi}} \dot{\boldsymbol{\Phi}}^2 \end{bmatrix} \right) \\
&+ \begin{bmatrix} +2\dot{\theta}_0 l \mathbf{K}^T \mathbf{C}_{\boldsymbol{\Phi}} \dot{\boldsymbol{\Phi}} + \dot{\theta}_0^2 * l \mathbf{K}^T \cos \boldsymbol{\Phi} + \ddot{\theta}_0 l \mathbf{K}^T \sin \boldsymbol{\Phi} \\ +2\dot{\theta}_0 l \mathbf{K}^T \mathbf{S}_{\boldsymbol{\Phi}} \dot{\boldsymbol{\Phi}} + \dot{\theta}_0^2 * l \mathbf{K}^T \sin \boldsymbol{\Phi} + \ddot{\theta}_0 l \mathbf{K}^T \cos \boldsymbol{\Phi} \end{bmatrix} + M_p \begin{bmatrix} \mathbf{e}^T \mathbf{f}_{D,t} \\ \mathbf{e}^T \mathbf{f}_{D,n} \end{bmatrix} + \begin{bmatrix} +v_n \dot{\theta}_0 \\ -v_t \theta_0 \end{bmatrix} \quad (1)
\end{aligned}$$

where  $M_p = \begin{bmatrix} nm + u_n \mathbf{e}^T \mathbf{S}_{\boldsymbol{\Phi}}^2, -u_n \mathbf{e}^T \mathbf{S}_{\boldsymbol{\Phi}} \mathbf{C}_{\boldsymbol{\Phi}} \\ -u_n \mathbf{e}^T \mathbf{S}_{\boldsymbol{\Phi}} \mathbf{C}_{\boldsymbol{\Phi}}, nm + u_n \mathbf{e}^T \mathbf{C}_{\boldsymbol{\Phi}}^2 \end{bmatrix}^{-1}$ . The torque equations for all links are expressed in matrix form as

$$\begin{aligned}
\mathbf{J} \ddot{\boldsymbol{\Phi}} + \mathbf{M}_{\boldsymbol{\Phi}} \dot{\boldsymbol{\Phi}} - \boldsymbol{\tau} + \mathbf{M}_{\boldsymbol{\Phi}} \mathbf{e} \ddot{\theta}_0 + \mathbf{W}_{\boldsymbol{\Phi}} \dot{\boldsymbol{\Phi}}^2 + \mathbf{W}_{\boldsymbol{\Phi}} \mathbf{e} \dot{\theta}_0^2 \\
+ 2\mathbf{W}_{\boldsymbol{\Phi}} \dot{\boldsymbol{\Phi}} \dot{\theta}_0 + \mathbf{K}_{Dt} \mathbf{f}_{Dt} + \mathbf{K}_{Dn} \mathbf{f}_{Dn} = \mathbf{D}^T \mathbf{u} \quad (2)
\end{aligned}$$

where  $M_{\Phi}$ ,  $W_{\Phi}$ ,  $K_{Dt}$ ,  $K_{Dn}$  are defined as

$$\begin{aligned} M_{\Phi} &= ml^2 S_{\Phi} V S_{\Phi} + ml^2 C_{\Phi} V C_{\Phi} + u_n l^2 K_1 K_1^T S_{\Phi} + u_n l^2 K_1 K_1^T C_{\Phi}, \\ W_{\Phi} &= ml^2 S_{\Phi} V C_{\Phi} + ml^2 C_{\Phi} V S_{\Phi} + u_n l^2 K_1 K_1^T C_{\Phi} - u_n l^2 K_2 K_2^T S_{\Phi}, \\ A_1 &= S_{\Phi} K S_{\Phi}^2 + C_{\Phi} K S_{\Phi} C_{\Phi}, K_{Dt} = u_n l^2 A_1 e e^T m11 - u_n l^2 A_2 e e^T m21 - l S_{\Phi} K, \\ K_1 &= A1 + u_n A_1 e e^T (m12 S_{\Phi} C_{\Phi} - m11 S_{\Phi}^2) - u_n A_2 e e^T (m22 S_{\Phi} C_{\Phi} - m21 S_{\Phi}^2), \\ K_2 &= A2 - u_n A_1 e e^T (m11 S_{\Phi} C_{\Phi} - m12 C_{\Phi}^2) + u_n A_2 e e^T (m21 S_{\Phi} C_{\Phi} - m22 C_{\Phi}^2), \\ A_2 &= S_{\Phi} K S_{\Phi} C_{\Phi} + C_{\Phi} K C_{\Phi}^2, K_{Dn} = u_n l^2 A_1 e e^T m12 - u_n l^2 A_2 e e^T m22 + l C_{\Phi} K. \end{aligned}$$

In summary, the equations of motion for the underwater eel robot are given by Eqs. (1) and (2). By introducing the state variables

$$\mathbf{x} = [\phi^T, \theta_0, p_x, p_y, \dot{p}_x, \dot{\theta}_0, \dot{\phi}^T, v_t, v_n]^T \in R^{2n+4}$$

the model of the Underwater Eel Robot in state space form is rewritten as  $\dot{\mathbf{x}} = \mathbf{f}(\mathbf{x}, u)$ . For further details, please see [17].

### 3 The Optimization Goal Description and Multi-objective Optimal Method

#### 3.1 Gait Patterns

There are many gaits for eel robot. Firstly, the definition of general gait is given.

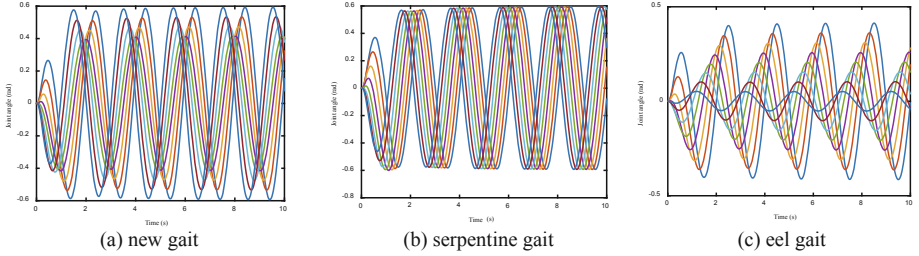


Fig. 2. Gait patterns.

$$\phi_j = \alpha g(n, i) \sin(\omega t + (j - 1)\beta) + \gamma \quad (3)$$

where gait amplitude  $\alpha$ , gait frequency  $\omega$ , and phase shift  $\beta$  are considered to decision variables. Different  $g(n, i)$  means different gait pattern. The phase offset  $\gamma$  control the direction of swimming. Figure 2 shows the pictures of all the joint angle varies with time in three gait patterns.

The new gait is a new gait pattern found in the tangential velocity tracking of eel robot based on iterative learning control [15]. See Fig. 2(a). This gait is

characterized by smaller amplitudes near the center of mass and larger amplitudes farther away from the center of mass. In our previous work [15], we found that new gait always occurs at high speed. The gait is defined as follows

$$\phi_j = \begin{cases} \alpha \frac{(n+2-j)}{(n+1)} \sin(\omega t + (j-1)\beta) + \gamma, j < n/2 \\ \alpha \frac{(2+j)}{(n+1)} \sin(\omega t + (j-1)\beta) + \gamma, j > n/2 \end{cases}$$

Serpentine gait is considered to have high propulsion efficiency and is the most commonly gait pattern in various literature [14, 16], see Fig. 2(b), is defined as follows.

$$\phi_j = \alpha \sin(\omega t + (j-1)\beta) + \gamma, j = 1 \dots n-1. \quad (4)$$

The eel gait is inspired by Bio-eel's swimming, see Fig. 2(c). This gait is characterized by smaller head amplitude and larger tail amplitude. Each joint angle is defined as follows

$$\phi_j = \alpha \frac{n-j}{n+1} \sin(\omega t + (j-1)\beta) + \gamma, j = 1 \dots n-1. \quad (5)$$

The new gait have not been analyzed in detail in previous literatures. There is no comparison between the advantages and disadvantages of the new gait compared to other gaits. Therefore, this paper analyzes the three gait patterns mentioned above. In these gaits, the same range of gait parameters can be constrained as follows.

$$0 \leq \alpha \leq 1.4, 0 \leq \omega \leq \pi, 0 \leq \beta \leq \pi.$$

Since the linear relationship between gait frequency  $\omega$  and velocity has been confirmed by most literatures, we mainly focus on the optimal distribution of the other two parameters.

### 3.2 Evaluation Indicator

The indicator to evaluate the gait efficiency is defined as

$$J_1 = \frac{P_{min}}{v_t} \quad (6)$$

where  $P_{min}$  is a function representing the input power of all joints.  $v_t$  is the velocity of robot.

The smaller the indicator  $J_1$ , the higher the efficiency. If the index is optimized directly, it is easy to cause the velocity to approach zero. Therefore, we decompose the indicator into two objectives, and then optimize it by multi-objective optimization algorithm. The optimal parameters  $\alpha, \beta, \omega$  are obtained under the objective of minimum input power and maximum speed. After the optimization is completed, this indicator is used to evaluate the efficiency. The input power of all joints is

$$P_{in} = \sum_{i=1}^{n-1} \tau \dot{\phi}$$

Different from other literature, this paper takes the sum of the maximum input power plus absolute value as the input power evaluation function, which can effectively prevent the situation of excessive instantaneous power. The specific optimization objective function is expressed as follows.

$$V_{\min} = - \max_{t \in [t_0, t_1]} \{v_t(t)\} \quad (7)$$

$$P_{\min} = \min_{i=1, \dots, n-1} \sum \left( \max_{t \in [t_0, t_1]} |\tau(t) \cdot \dot{\phi}(t)^T| \right) \quad (8)$$

where  $v_t$  is the tangential velocity of eel-like robot. The initial time and end time are represented by  $t_0, t_1$  respectively.  $\tau(t)$  is the input joint torque.  $\dot{\phi}$  is the joint angular velocity. Vector dot product is denoted by  $\cdot$ .

It is necessary to select a multi-objective optimization algorithm which can converge to the pareto surface quickly due to the complexity of the dynamics and the long time to obtain numerical solutions. In this paper, NSGA-II algorithm is used to optimize the parameters of eel-like robot. This algorithm does not require initial values and can reach the optimal solution at a faster speed. It is a non-dominated sorting genetic algorithm with elite strategy, which can obtain Pareto surface faster for complex models. The non-dominated sorting genetic algorithm NSGA-II is proposed based on the Pareto sorting idea.

## 4 Simulation and Experiment

The dynamics was calculated using ode45 solver in Matlab with a relative and absolute error tolerance of  $10^{-6}$ , and the number of modules  $n$  is set to 8. The control gain of the PD controller in the simulation is designed as  $K_p = 200, K_d = 100$ . Initial states are set to zero. The NSGA-II algorithm used a crossover probability of 0.9, a mutation probability of 0.1, a population of 200, and an evolutionary algebra of 200.

The fluid parameters were set as  $\rho = 1000 \text{ kg/m}^3, C_M = 1, C_f = 0.03, C_D = 2, C_a = 1, \lambda_1 = 7.1905 \times 10^{-4}, \lambda_2 = 1.5 \times 10^{-3}, \lambda_3 = 7.1526 \times 10^{-5}$ . For a cylindrical body immersed in a flow with a Reynolds number of approximately  $Re = 10^5$ . The normal drag coefficient for the environmental force was set to  $c_n = 9.3750$ , and the tangential drag coefficient was set to  $c_t = 0.2209$ , and the added mass coefficient was set to  $u_n = 0.5522, u_t = 0$ .

### 4.1 Analysis of Optimization Results

According to Pareto set obtained by NSGA-II, it is found that optimal phase shift of eel gait is near 0.5 rad, and the optimal amplitude of eel gait is mainly around 0.5 rad. Optimal phase shift of serpentine gait is near 0.5 rad, and the optimal amplitude serpentine gait is mainly 0.1–0.5 rad. The optimization results of serpentine gait are consistent with the paper [12, 13]. The optimal phase shift of new gait is also near 0.5 rad.

The optimization results are shown in Fig. 3, which describe the relationship between the optimized velocity and the input power of the three gait pattern.

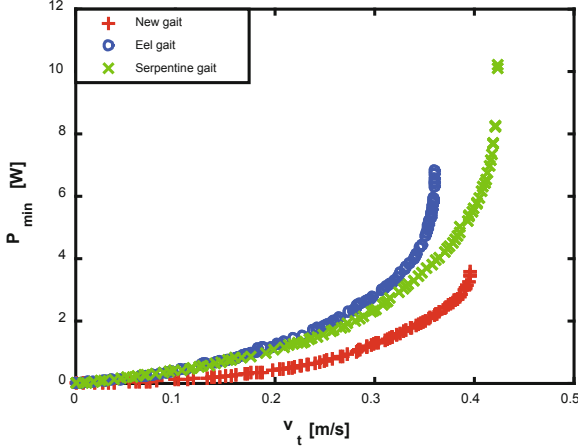


**Fig. 3.** Velocity vs input power.

In Fig. 3, the points corresponding to the same velocity of those gait patterns are taken, and the corresponding efficiency of each gait are obtained in Table 2. Eel-like robot with the new gait has smaller input power at the same speed. At the same input power, eel-like robot with the new gait has faster speed. It can be seen that the new gait is more efficient ( $J_1$  is smaller). Although the new gait has higher energy efficiency, its maximum speed can only reach 0.3961 m/s. More higher speed can be provided by the serpentine gait.

**Table 2.** Optimal gaits and corresponding gait parameters

Gait	$v_t/(m/s)$	$P_{min}/(W)$	$\alpha$	$\beta$	$\omega$	$J_1$
Serpentine gait	0.299	2.342	0.265	0.329	1.857	7.83
Eel gait	0.297	2.76	0.413	0.553	3.064	9.293
New gait	0.299	1.242	0.367	0.388	1.931	4.154

In summary, compared with serpentine gait and eel gait, the new gait consumes less power at the same speed and has faster speed at the same input power. Compared with serpentine gait and eel gait, the new gait has higher swimming efficiency. Next, the serpentine gait and the new gait will be analyzed in detail.

## 4.2 Simulation and Experimental Analysis

In order to analyze the efficiency of serpentine gait and new gait, and the influence of amplitude and phase shift on velocity. This section uses the 3D motion capture system VXtrace to obtain real-time location. All the experimental equipment is shown in Fig. 4. Motion capture system VXtrace is composed of C-trace

scanner, Calibration rod, Maxshot and Controller. The system can accurately and timely measure the position and direction of the reflecting target in space. The visual range of C-Track 780 is  $7.8\text{ m}^3$ , the horizontal visual range is trapezoidal, and the sampling frequency of C-Track 780 is set to 29 Hz.



Fig. 4. Experimental equipments.

The robot consists of 8 modules, the total length is 1.6 m and the total mass is 6.75 Kg (see Fig. 5). The robot is completely submerged in water, and the robot moves in the horizontal plane. O-ring and silicone are used to ensure the sealing of the robot. Each modular universal unit MUU has two degrees of freedom of pitch and yaw.



Fig. 5. The underwater eel robot.

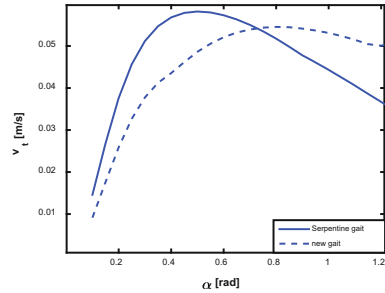


Fig. 6. Velocity vs amplitude.

In order to obtain the forward velocity of the robot, the Savitzky-Golay filter in MATLAB is used to estimate the velocity of the robot. The window length of the filter is set to 19, and the mean filter method is used when the filter is invalid. The most important feature of this filter is that it can keep the shape and width of the signal unchanged while filtering out the noise. In addition, the initial state of the experiment is consistent.

**Velocity Vs Amplitude.** In Fig. 6, the simulation of the two gaits is obtained by changing the amplitude under the condition of constant frequency (0.5 Hz) and phase (0.8 rad). The simulation results show that speed of both gaits increases and then decreases with the increase of the amplitude. The new gait and serpentine gait exists the optimal amplitude to maximize the velocity. After repeated experiments, these points near the optimal amplitude of the serpentine gait and new gait are selected as Tables 3 and 4. Table 4 shows that in the new gait, as the increase of the amplitude, the power consumption  $P_{in}$  increases, the average power increases, the swimming efficiency decreases ( $J_1$  increases), and there is an optimal amplitude to maximize the average speed of the experiment. Compared to Table 3 and 4, At the same input power, the experimental average speed of serpentine gait is lower than that of new gait, and the average input power of new gait is lower than that of serpentine gait (except for  $\alpha = 0.8$ ). When the average speed is the same, the  $J_1$  of the new gait is lower than that of the serpentine gait, so the efficiency of the new gait is higher. There is a slight difference between the individual results of the experiment ( $\alpha = 0.8$ ) and the simulation results. The possible reason is that the robot was subject to extra resistance produced by dragging of wires due to the large swing of the tail. In addition, the actual shape different from the simulation hypothesis. In fact, the simulation model can not fully reflect some characteristics of the actual prototype. For example, the simulation robot is completely symmetrical, while the robot prototype is not completely symmetrical. The simulation assumes that the cross-section of the prototype is a cylinder, while the actual cross-section of the prototype is not a complete cylinder.

**Table 3.** Simulation and experimental of serpentine gait

$\alpha/(rad)$	Average power/(W)	Average speed/(m/s)	$J_1$
0.5	0.0193	0.0197	0.9797
0.6	0.0244	0.0234	1.0427
0.7	0.0304	0.0208	1.4615
0.8	0.0375	0.0258	1.4535

**Table 4.** Simulation and experimental of new gait

$\alpha/(rad)$	Average power/(W)	Average speed/(m/s)	$J_1$
0.5	0.0149	0.0179	0.8324
0.6	0.0190	0.0197	0.9645
0.7	0.0235	0.0242	0.9711
0.8	0.0285	0.0178	1.6011

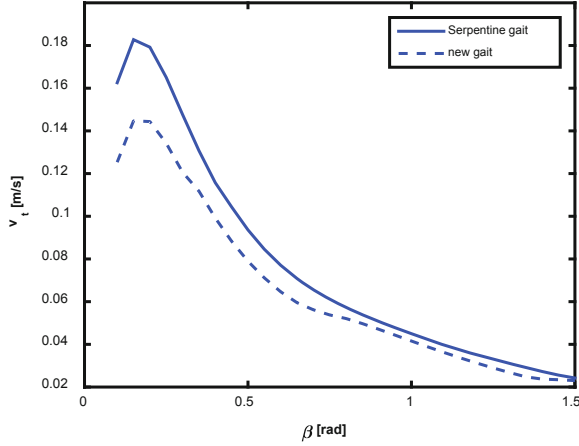


**Fig. 7.** Velocity vs phase shift.

**Velocity vs Phase Shift.** The influence of phase shift on velocity is analyzed by changing phase shift under the condition of constant amplitude (0.6 rad) and frequency (0.5 Hz). The variation trend of velocity with phase shift is shown in Fig. 7. It can be seen that the phase shift between the two gaits also has an optimal value (near 0.2–0.3 rad). Several points are selected from the figure, and the experimental result of the serpentine gait and new gait are shown in Tables 5 and 6 respectively. The average power is decreasing with the increase of phase shift by analysing the Tables 5 and 6. In addition, as the phase shift increases, the indicator  $J_1$  of the new gait decreases, and the efficiency of the new gait increases. Comparing simulation and experiment, it is found that optimal phase of the new gait and the serpentine gait exists for maximum speed. Overall, the experimental results are consistent with the optimization results of the NSGA-II algorithm.

**Table 5.** Simulation and experimental of serpentine gait

$\beta/(rad)$	Average power/(W)	Average speed/(m/s)	$J_1$
0.3	0.1842	0.0287	6.4181
0.4	0.1380	0.0256	5.3906
0.5	0.0905	0.0284	3.1866
0.6	0.0554	0.0270	2.0519
0.7	0.0346	0.0218	1.5872
0.8	0.0244	0.0234	1.0427

**Table 6.** Simulation and experimental of new gait

$\beta/(rad)$	Average power/(W)	Average speed/(m/s)	$J_1$
0.3	0.1181	0.0323	3.6563
0.4	0.0734	0.0309	2.3754
0.5	0.0411	0.0254	1.6181
0.6	0.0257	0.0257	1.0000
0.7	0.0211	0.0219	0.9635
0.8	0.0190	0.0197	0.9645

## 5 Conclusions

The optimal gait parameter combination of three different gait patterns was analyzed by multi-objective optimization algorithm NSGA-II to obtain high efficiency swimming gait, and the swimming efficiency of three gait patterns was evaluated by efficiency indicator  $J_1$ . The simulation results show that the new gait has faster speed at the same input power, and consumes less input power at the same speed. That is, the new gait has higher swimming efficiency than the serpentine gait and eel gait. Then, experiments are carried out to verify that the new gait is more efficient. In addition, optimal gait amplitude and the optimal phase shift exist that make the velocity maximum in both the new gait and the serpentine gait. In future research, we will analyze the influence of additional resistance caused by dragging wires.

## References

1. Wiens, A.J., Nahon, M.: Optimally efficient swimming in hyper-redundant mechanisms: control, design, and energy recovery. *Bioinspir. Biomim.* **7**(4), 046016 (2012)
2. Ostrowski, J.P., Desai, J.P., Kumar, V.: Optimal gait selection for nonholonomic locomotion systems. *Int. J. Robot. Res.* **19**(3), 225–237 (1999)
3. Tesch, M., Schneider, J., Choset, H.: Expensive multiobjective optimization for robotics. In: *IEEE International Conference on Robotics and Automation*, pp. 973–980. IEEE (2013)
4. Guo, X., Ma, S., Li, B., Wang, M., Wang, Y.: Optimal turning gait for a three-link underwater robot. In: *2015 IEEE International Conference on Cyber Technology in Automation, Control, and Intelligent Systems, IEEE-CYBER 2015*, pp. 1321–1326 (2015)
5. Kohannim, S., Iwasaki, T.: Optimal turning gait for mechanical rectifier systems with three dimensional motion. In: *53rd IEEE Conference on Decision and Control*, pp. 5862–5867 (2014)
6. Reviewed, P., Oscillations, O.: *Optimal Oscillations and Chaos Generation in Biologically-Inspired Systems*. University of California Los Angeles (2016)
7. Kansa, E., Marsden, J.E.: Optimal motion of an articulated body in a perfect fluid. In: *Proceedings of the 44th IEEE Conference on Decision and Control, and the European Control Conference, CDC-ECC 2005* (2005)

8. van Rees, W.M., Gazzola, M., Koumoutsakos, P.: Optimal morphokinematics for undulatory swimmers at intermediate Reynolds numbers. *J. Fluid Mech.* **775**, 178–188 (2015)
9. Crespi, A., Ijspeert, A.J.: Online optimization of swimming and crawling in an amphibious snake robot. *IEEE Trans. Robot.* **24**(1), 75–87 (2008)
10. Corts, J.: Optimal gaits for dynamic robotic locomotion. *Int. J. Robot. Res.* **20**(9), 707–728 (2001)
11. Parodi, O., Lapierre, L., Jouvencel, B.: Optimized gait generation for Anguilliform motion. In: *OCEANS 2006 - Asia Pacific*, pp. 1–8 (2006)
12. Wei, W., Deng, G.Y.: Optimization and control of NSGA-II in snake like robot. *Comput. Eng.* **38**(8), 137–140 (2012)
13. Mehta, V.: Optimal gait analysis of snake robot dynamics. *Coe. Psu. Edu.* (2007)
14. Kelasidi, E., Pettersen, K.Y., Gravdahl, J.T.: Energy efficiency of underwater snake robot locomotion. In: *Control and Automation*, pp. 1124–1131. *IEEE* (2015)
15. Zhang, A., Ma, S., Li, B., Wang, M.: Tracking control of tangential velocity of eel robots based on iterative learning control. *Robot* **40**(06), 3–12 (2018)
16. Lapierre, L., Jouvencel, B.: Path following control for an eel-like robot. In: *Europe Oceans 2005*, Brest, France, vol. 1, no. 1, pp. 460–465 (2005)
17. Zhang, A., Ma, S., Li, B., Wang, M., Wang, Y.: Modeling and simulation of an underwater planar eel robot in non-inertial frame. In: *The 7th Annual IEEE International Conference on CYBER Technology in Automation, Control, and Intelligent Systems* (2016)